Evaluating consistency between total column CO_2 retrievals from OCO-2 and the *in-situ* network over North America: Implications for Carbon flux estimation

Bharat Rastogi[1,2], John B Miller[2], Micheal Trudeau[1,2], Arlyn E Andrews[2], Lei Hu[1,2], Marikate Mountain[3], Thomas Nehrkorn[3], John Mund[2], Kaiyu Guan[4], and Caroline B Alden[1,2]

[1]Cooperative Institute for Research in Environmental Sciences (CIRES), University of Colorado Boulder, CO, 80309
[2]Global Monitoring Laboratory, National Oceanic and Atmospheric Administration, Boulder, CO 80305
[3]Atmospheric and Environmental Research, Lexington, MA 02041
[4]Department of Natural Resources and Environmental Sciences, College of Agriculture, Consumer, and Environmental Sciences, University of Illinois at Urbana-Champaign, Urbana, IL 60801

Correspondence: Bharat Rastogi (bharat.rastogi@noaa.gov)

Abstract. Feedbacks between the climate system and the carbon cycle represent a key source of uncertainty in model projections of Earth's climate, in part due to our inability to directly measure large scale biosphere-atmosphere carbon fluxes. *In-situ* measurements of CO_2 mole fraction from surface flasks, towers and aircraft are used in inverse models to infer fluxes, but mea-

5 surement networks remain sparse, with limited or no coverage over large parts of the planet. Satellite retrievals of total column CO_2 (X_{CO_2}), such as those from NASA's Orbiting Carbon Observatory-2 (OCO-2), can potentially provide unprecedented global information about CO_2 spatiotemporal variability. However, for use in inverse modeling, data need to be extremely stable, highly precise and unbiased to distinguish abundance changes emanating from surface fluxes from those associated with variability in weather. Systematic errors in X_{CO_2} have been identified and, while bias correction algorithms are applied

10 globally, inconsistencies persist at regional and smaller scales that may complicate or confound flux estimation. To evaluate X_{CO_2} retrievals and assess potential biases, we compare OCO-2 *v10* retrievals with *in-situ* data-constrained X_{CO_2} simulations over North America estimated using surface fluxes and boundary conditions optimized with observations that are rigorously calibrated relative to the WMO X2007 CO_2 scale. Systematic errors in simulated atmospheric transport are independently evaluated using unassimilated aircraft and AirCore profiles. We find that the global OCO-2 *v10* bias correction shifts the distri-

15 bution of retrievals closer to the simulated X_{CO_2}, as intended. Comparisons between bias corrected and simulated X_{CO_2} reveal differences that vary seasonally. Importantly, the difference between simulations and retrievals is of the same magnitude as the imprint of recent surface flux in the total column. This work demonstrates that systematic errors in OCO-2 *v10* retrievals of X_{CO_2} over land can be large enough to confound reliable surface flux estimation and that further improvements in retrieval and bias correction techniques are essential. Finally, we show that independent observations, especially vertical profile data, such

20 as from NOAA's aircraft and AirCore programs are critical for evaluating errors in both satellite retrievals and carbon-cycle models.

1 Introduction

Interannual variability in the growth rate of atmospheric CO_2 is largely driven by variability in uptake and release by terrestrial
ecosystems (Heimann and Reichstein, 2008; Piao et al., 2020). Oceanic fluxes also respond to variability in climate (e.g.,
DeVries et al., 2019; Riebesell et al., 2009), but the amplitude of oceanic flux variability is thought to be considerably less than
for terrestrial fluxes. While individual component fluxes (e.g., photosynthesis) are currently not directly measurable at scales
larger than leaf or soil chambers, well-calibrated and precise measurements of CO_2 have allowed us to track the accumulation
of this greenhouse gas in the atmosphere and associated radiative feedbacks on the global climate, as well as its spatiotemporal
variability (e.g., Tans et al., 1989). These measurements continue to provide valuable insights into surface flux processes and
feedbacks (e.g., Tans et al., 1990; Ballantyne et al., 2012; Keeling et al., 2017; Arora et al., 2020). Observed spatial and
temporal gradients in CO_2 mole fraction (relative to dry air) can be combined with a numerical model of atmospheric transport
to infer surface fluxes (i.e. exchange of CO_2 between the atmosphere and the underlying ocean or land surface), in a "top-
down" or inverse modelling framework (e.g., Peters et al., 2007; Gurney et al., 2002). An ever-increasing global greenhouse
gas measurement network and progress in modelling techniques have tremendously improved our understanding of surface
processes. However, measurement networks remain sparse and continue to under-sample large parts of the world, including
large parts of North America, which can limit our understanding of surface flux processes in those regions. Furthermore,
incompatibility across datasets that arises from inconsistent calibrations or systematic errors can significantly corrupt surface
flux estimates – leading to inaccurate models of carbon-climate interactions and subsequent errors in climate forecasts.

Satellite retrievals of total column CO_2 mole fraction (X_{CO_2}), such as those from NASA's Orbiting Carbon Observatory-2
(OCO-2), have the potential to provide unprecedented information about spatio-temporal patterns and variability in the Earth's
atmosphere. However, space-based observations of X_{CO_2} must be extremely stable, highly precise and free from bias to detect
and quantify abundance changes caused by a change in surface fluxes (Rayner and O'Brien, 2001; Olsen, 2004; Miller et al.,
2007; Houweling et al., 2003). This is critical, as even large surface flux signals are substantially diluted in the total column
and largely obscured by meteorological variability (Basu et al., 2018; Feng et al., 2019).

In-situ measurements that comprise global networks, such as NOAA's Global Greenhouse Reference Network (https://www.
esrl.noaa.gov/gmd/ccgg/ggrn.php), are rigorously evaluated and carefully calibrated relative to the World Meteorological Or-
ganization (WMO) calibration scale (data used here are reported on the X2007 scale), thus ensuring the fidelity of these
measurements over timescales of seasons to decades (Andrews et al., 2014; Hall et al., 2020). The "open-path" nature of space-
based X_{CO_2} measurements however, does not allow for direct calibration. Satellite retrievals of X_{CO_2} require complicated
models of atmospheric radiation and are sensitive to a host of assumptions about aerosols, clouds, interference of jointly re-
trieved parameters, surface properties and details of the instrumentation (Kulawik et al., 2019). Moreover, sensors typically
degrade over time, and limited information is available to characterize resulting time-dependent systematic errors. Post-launch

data corrections are performed if and when biases (O'Dell et al., 2018) and errors (Kiel et al., 2019) are identified, but are
55 severely limited due to the sparsity of calibrated *in-situ* vertical profile observations.

Currently, satellite derived $X_{\mathrm{CO_2}}$ retrievals are linked to the WMO scale most directly through a limited set of *in-situ* profiles
obtained over a network of ground-based Fourier Transform Infrared Spectrometers that comprise the Total Carbon Column
Observation Network (TCCON; Wunch et al., 2017). However, TCCON itself provides remotely sensed information about
$X_{\mathrm{CO_2}}$, and TCCON retrievals undergo a complex validation and bias correction routine (Wunch et al., 2010) that links these
60 retrievals to the WMO scale. Moreover, TCCON sites are few. Issues with validation of OCO-2 retrievals via TCCON have
been identified- seasonal and site-dependent biases have been reported (Wunch et al., 2017, 2015), raising questions about the
adequacy of this network to validate satellite derived $X_{\mathrm{CO_2}}$ products (Basu et al., 2013). This is especially important since sys-
tematic bias corrections of $X_{\mathrm{CO_2}}$ from TCCON data are developed over small spatio-temporal scales and extrapolated globally
(Wunch et al., 2011) for retrievals over land and ocean respectively (O'Dell et al., 2018). OCO-2 retrievals are additionally cor-
65 rected for bias by comparing with 4-D $\mathrm{CO_2}$ mole fraction fields from global inverse models, and a small-area approximation,
but both methods are prone to smoothing across fine-scale variability in $X_{\mathrm{CO_2}}$ (O'Dell et al., 2018; Corbin et al., 2008). While
bias correction generally reduces inferred surface flux uncertainty when retrievals are assimilated in atmospheric inversions
(Basu et al., 2013), even small retrieval errors can lead to large errors in inferred flux (Takagi et al., 2014; Chevallier et al.,
2014). Biases in $X_{\mathrm{CO_2}}$ from OCO-2, hereafter $X_{\mathrm{CO_2}}^{ret}$, have been identified, and found to be related to surface (e.g. pressure,
70 albedo) and atmospheric (e.g. aerosol loading, sky condition) properties (Kiel et al., 2019). However, systematic biases not
accounted for in the *v10* bias correction approach persist and therefore the measurement uncertainty associated with individual
retrievals is believed to be at least twice the value currently reported in the OCO-2 data files (Eldering et al., 2017).

Thus, a dynamic method to routinely evaluate satellite retrievals is necessary. In this study, we propose such a method that
takes advantage of the relatively dense *in-situ* network of $\mathrm{CO_2}$ mole fraction measurements over North America, and leverage
75 an ensemble of optimized flux estimates derived using the high resolution CarbonTracker-Lagrange $\mathrm{CO_2}$ inverse modeling
framework (Hu et al., 2019). We demonstrate an approach for constructing $X_{\mathrm{CO_2}}$ that offers optimal consistency with *in-situ*
measurements of $\mathrm{CO_2}$ dry air mole fraction calibrated relative to the WMO X2007 scale (Hall et al., 2020). We compare
our simulated $X_{\mathrm{CO_2}}$ retrievals with the *v10* OCO-2 product, evaluate the extent to which observed differences are consistent
with rigorous uncertainties on the simulated fields, and potentially correct biases in satellite retrievals. We essentially use the
80 CarbonTracker-Lagrange modeling framework to interpolate the existing *in-situ* measurements to the time and location of
OCO-2 retrievals. The *in-situ* measurement uncertainty is generally $\sim$ 0.15 [ppm] (Andrews et al., 2014), and we have
carefully accounted for uncertainty in regional boundary conditions and uncertainties in the optimized fluxes. While a single
realization of the simulated atmospheric transport is used here (a limitation of the approach that we aim to address in future
work by using transport ensembles), we evaluate transport uncertainty using independent vertical *in-situ* profiles of $\mathrm{CO_2}$.
85 CarbonTracker-Lagrange simulations are driven by meteorological simulations from the Weather Research Forecast model
system optimized for particle dispersion modeling (Nehrkorn et al., 2010) with resolution of 10 [km] over continental U.S.,
and 30 [km] over the rest of North America, considerably higher than global *in-situ* informed simulations that have so far
been used for OCO-2 evaluation (Kiel et al., 2019; Crowell et al., 2019; Miller and Michalak, 2020). Simulated $X_{\mathrm{CO_2}}$ are
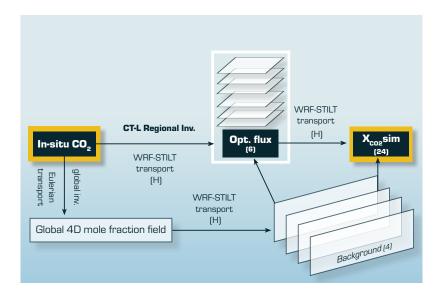
Figure 1. Flowchart linking *in-situ* measurements of CO_2 to simulated columns.

compared with OCO-2 *v10* retrievals, both before and after global bias correction, thus providing an independent evaluation of

90 the global bias correction over North America. In principle, differences can result from errors in the retrievals or from errors in

the CarbonTracker-Lagrange modeling framework, but we show that for certain seasons these differences are unlikely to result

from the latter. North America is a useful test-bed for evaluating consistencies and for developing improved model simulations

and retrieval bias correction strategies, given the relatively dense sampling network (compared to other regions) and that the

best surface flux estimates are likely to come from approaches that combine *in-situ* measurements and satellite retrievals (Basu

95 et al., 2013; Fischer et al., 2017; Byrne et al., 2020). The US Inter-Agency North American Carbon Program (Wofsy et al.,

2002) has supported intensely focused research for nearly two decades and has resulted in a wealth of datasets and model:data

fusion activities that have informed model development.

2 Methods

Simulated $X_{\mathrm{CO_2}}$, hereafter "$X_{\mathrm{CO_2}}^{sim}$", is constructed by estimating impact of different surface fluxes ($\Delta_{CO_2}^{flux}$) on the total column.

100 This involves imposing a time, latitude, longitude, and altitude dependent lateral boundary condition or background, which

accounts for changes in $X_{\mathrm{CO_2}}^{sim}$ originating outside our model domain. The chain of events that link the *in-situ* data with the

simulations is shown in fig. 1. We use multiple ensembles of surface flux and boundary conditions to assess uncertainty in each.

Comparisons with independent unassimilated aircraft and AirCore profiles are used to assess combined random and systematic

errors in surface flux, background and atmospheric transport.

2.1 Convolution Method

We follow the recommended protocol for comparing satellite retrievals with modeled CO_2 columns from the Atmospheric CO_2 Observations from Space (ACOS) retrieval algorithm (O'Dell et al., 2012).

$$X_{CO_2}^{sim} = \sum_{i=1}^{N} w_i \left[a_i . \chi_{CO_2,i}^{model} + (1 - a_i) . \chi_{CO_2,i}^{pri} \right] \tag{1}$$

Here, $X_{CO_2}^{sim}$ [ppm], the total column CO_2, is computed as a *pressure weighted* sum of the modeled column ($X_{CO_2}^{model} = \sum_{i=1}^{N} w_i . \chi_{CO_2,i}^{model}$), comprising N model (i.e., not OCO-2) levels from the surface to the top of the atmosphere (0.01 [hPa]). $\chi_{CO_2}^{model}$ is convolved with the OCO-2 averaging kernel profile (a_i) and the OCO-2 prior profile ($\chi_{CO_2}^{pri}$) and summed according to a pressure weighting function (w; identical to h in Connor et al., 2008). w is calculated as:

$$w = \sum_{i=1}^{N} w_i = \sum_{i=1}^{N} \left| \left(-p_i + \frac{p_{i+1} - p_i}{ln(\frac{p_{i+1}}{p_i})} \right) + \left(-p_i + \frac{p_i - p_{i-1}}{ln(\frac{p_i}{p_{i-1}})} \right) \right| \frac{1}{p_{surf}}, \tag{2}$$

where p_i and p_{surf} are WRF modeled pressure at level i and at the surface respectively. The profile sum of w is always unity.

$\chi_{CO_2,i}^{model}$ [ppm] is constructed as:

$$X_{CO_2}^{model} = \sum_{i=1}^{N} \chi_{CO_2,i}^{bkg} + \sum_{i=1}^{N-3} \Delta_{CO_2,i}^{flux} \tag{3}$$

Here, $\chi_{CO_2,i}^{bkg}$ [ppm] represents background (i.e., lateral boundary condition, described in sec. 2.4) and $\Delta_{CO_2,i}^{flux}$ [ppm] denotes the impact of surface flux at level i of the column. $\Delta_{CO_2,i}^{flux}$ is computed at discrete levels from the surface to 14 [km], whereas $\chi_{CO_2,i}^{bkg}$ is computed at 3 additional levels. These additional levels represent the upper troposphere and the stratosphere, where influence of recent surface flux is assumed to be zero. $\Delta_{CO_2,i}^{flux}$ is estimated as:

$$\Delta_{CO_2,i}^{flux} = H_i(s_{bio} + s_{ff} + s_{bmb} + s_{ocn}), \tag{4}$$

where H_i [ppm $CO_2.(\mu\,mol\,m^{-2}\,s^{-1})^{-1}$] represents the sensitivity at pressure level i of simulated X_{CO_2} to upwind surface fluxes (detailed in sec. 2.3), and s indicates surface flux [$\mu\,mol\,m^{-2}\,s^{-1}$]. s_{bio} denotes net ecosystem exchange (i.e. the sum of ecosystem photosynthesis and respiration), s_{bmb} denotes biomass burning, s_{ff} corresponds to fossil fuel emissions and s_{ocn} is the net ocean-atmosphere flux. Fluxes are described in detail in sec. 2.5.

2.2 OCO-2 retrievals and receptor selection criterion

We construct X_{CO_2} for valid *land-nadir* and *land-glint* $X_{CO_2}^{ret}$ from the *v10* data product (Osterman et al., 2020) over North America between September 2014 and August 2015. Globally, OCO-2 retrievals are primarily obtained in three operation
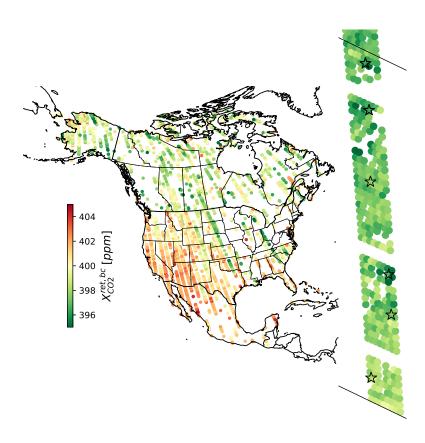
130   modes: Land Glint, Land Nadir, and Ocean Glint. Additionally, retrievals are obtained in "target" mode, for evaluation against
TCCON, and a "transition" mode, where the sensor switches between modes. While the "nadir" mode is mostly used over
land, over darker ocean the satellite sensor is able to receive a higher fraction of directly reflected sunlight in a separate "glint"
mode (Eldering et al., 2017). Here, we evaluate soundings over land obtained in both *nadir* and *glint* modes. Additionally, only
retrievals that passed the aerosol and cloud-screening filers are considered (i.e., quality flagged as 0, or "good").

135   Over North America, there can be a few thousand to tens of thousands of valid retrievals on any given day (Fig. 2a).
Each retrieval covers an area of approximately $1.29 \, [km] \times 2.25 \, [km]$ on the surface. Individual satellite retrievals are known
as *footprints*. The satellite collects 8 simultaneous *footprints*, and the next row of *footprints* are spaced $300 \, [ms]$ apart. For
each satellite overpass (*along-track*), we select locations every $2 \, [s]$ over the continental U.S. (i.e.,$\sim 12 \, [km]$) and $4 \, s$ (i.e.,$\sim$
$24 \, [km]$) over the rest of North America (Fig. 2b). These locations are usually called receptors in a Lagrangian particle dis-

140   persion model (LPDM) as they represent locations and times from which a set of particles are released and tracked back in
time. In an LPDM, an ensemble of particles is released from each receptor, and the residence time of particles in the planetary
boundary layer is used to calculate sensitivities describing the relationship between upwind surface fluxes and mole fraction
at the receptor location. Ultimately, a library of sensitivity arrays is generated corresponding to X_{CO_2} retrieval locations. Note
that these sensitivity arrays are sometimes called footprints or influence functions. Here we avoid this use of footprints so as

145   not to create confusion with OCO-2 footprints (i.e. scenes). This method enables improved simulation of *near-field* transport
compared to Eulerian gridded models, as particle locations are not restricted to grid-boxes and meteorological fields can be
interpolated to sub-grid scale locations (Lin et al., 2003), and has been used extensively in estimating regional trace gas fluxes
in inverse models using *in-situ* measurements (e.g., Schuh et al., 2009; Gourdji et al., 2012; Lauvaux et al., 2013; Alden et al.,
2016; Hu et al., 2019).

150   In this study, a vertical profile of receptors corresponding to a range of altitudes is created corresponding to the location of a
single valid satellite retrieval. We preferentially select receptors that are in the middle of the OCO-2 *track* to provide the most
spatially representative sample and minimize footprint dependant biases (O'Dell et al., 2012). For this analysis, we assume that
$X_{CO_2}^{sim}$ from a given receptor location is representative of all $X_{CO_2}^{ret}$ within $1 \, [s]$. $\sim 32,000$ unique receptor profiles associated
with valid retrievals are created between September 2014 and August 2015 representing ~ 1.61 million retrievals that passed

155   quality flags between September 2014 and August 2015. At each receptor, 24 unique $X_{CO_2}^{sim}$ are created, from combinations of
six flux and four background ensemble members (Fig. 1). Using an ensemble of 24 flux-background combinations provides an
estimate of unresolved variability in the simulations. In this analysis we report $X_{CO_2}^{sim}$ as the the mean and standard deviation
of these simulations. Similarly, $X_{CO_2}^{ret}$ represents the mean of all OCO-2 footprints within $\pm 1 \, [s]$ for a selected retrieval.

A profile of receptors for each selected satellite scene consists of discrete altitude levels approximately representing the

160   lowermost $850 \, [hPa]$ of the atmosphere. Models sampled for background estimation are sampled at receptor locations to
account for the rest of the column (detailed in sec. 2.4). A similar method (the application of a regional Lagrangian model
to estimate source-receptor relationships) was developed recently by Wu et al. (2018). In that study a set of model particles
distributed throughout an entire column of air (weighted to appropriately represent the retrieved total column, i.e., "the column
receptor") was transported and tracked backward in time and a single surface flux sensitivity array was computed for the total

Figure 2. All valid satellite retrievals for June 2015 (left). A zoomed-in map (right) shows all retrievals for a section of an individual sounding and locations of *along-track* receptors (stars). Black lines in the zoomed map indicate 1° latitude bands.

165   column. In contrast, here we establish source-receptor relationships at discrete altitude intervals and then apply appropriate vertical weighting for the column. This method has a higher computational cost and results in larger output files but adds flexibility in the simulation, for instance, a quick recalculation can be performed if the OCO-2 averaging kernel is modified and more importantly, our simulated profiles can be used with experimental retrieval products such as partial column retrievals (e.g., Kulawik et al., 2017).

170   **2.3   Transport model and constructing column weighted surface-sensitivity arrays: H**

We use output from the Stochastic Time-Inverted Lagrangian Transport (STILT) particle dispersion model (Lin et al., 2003) driven with high resolution meteorological fields from a customized implementation of the Weather Research and Forecasting (WRF) model (Nehrkorn et al., 2010). We use the WRF-STILT modeling configuration developed for the CarbonTracker-Lagrange modeling framework (Hu et al., 2019).

Atmospheric
Chemistry
and Physics
Discussions

175   The high spatial resolution of regional models provides an appropriate framework to investigate relatively fine-scale structure in atmospheric transport (e.g. mesoscale) and atmospheric signatures of surface flux heterogeneity. WRF model fields are computed at $10\,[km]$ spatial resolution over temperate North America and $30\,[km]$ spatial resolution outside of temperate North America. STILT is run off-line (i.e. driven by archived hourly WRF output) and trajectories are computed backwards in time from each receptor location. STILT surface-sensitivity arrays represent simulated upwind surface flux influence for 10

180   days prior to each observation at $1° \times 1°$ spatial and 1 hourly temporal resolution. A library of WRF-STILT surface-sensitivity arrays is pre-computed, archived, and can be efficiently convolved with independently estimated surface fluxes. This is in contrast to most modern Eulerian model CO_2 simulations, where the transport model needs to be rerun whenever a new surface flux product becomes available. STILT surface-sensitivity arrays have units of $[ppm(\mu\,mol\,m^{-2}\,s^{-1})^{-1}]$.

The OCO-2 retrieval is a *pressure-weighted* mean of χ_{CO_2} obtained at 20 equally spaced pressure boundaries from the

185   surface to the top of the atmosphere. STILT receptors however, are specified not on the pressure grid used for OCO-2 retrievals, but at fixed altitudes above ground level and with high vertical resolution where strong gradients in CO_2 are expected (e.g. near the surface, or at the top of planetary boundary layer). Additionally, $X_{CO_2}^{ret}$ is computed from a combination of the signal received by the spectrometer and an *a priori* profile ($\chi_{CO_2}^{pri}$). This approach constrains the uppermost portion of the atmospheric column where the satellite sensor lacks sensitivity. The relative weights of the received signal and $\chi_{CO_2}^{pri}$ are described by the

190   column averaging kernel (a; O'Dell et al., 2012), which is computed during the retrieval and archived along with $X_{CO_2}^{ret}$ and $\chi_{CO_2}^{pri}$. Thus, the first step in creating column-weighted surface-sensitivity arrays (H) is to interpolate $\chi_{CO_2}^{pri}$ and a onto the STILT grid. Then, a pressure weighting function (eq. 2) is applied to appropriately weight the surface sensitivity obtained from all receptors for each column. The upper $150\,[hPa]$ of the atmosphere is considered as part of the lateral boundary condition (the column weighted background; section 2.4), as sensitivity to recent surface flux is assumed to be zero at these pressure

195   levels and the WRF-STILT framework has not been optimized for upper atmospheric simulations.

2.4   Column weighted background: $X_{CO_2}^{bkg}$

The background or lateral boundary condition is an essential component of regional models, required to isolate changes in CO_2 from surface fluxes within the model domain. Boundary values need to represent synoptic variability and contributions from surface fluxes outside the model domain and may contribute significantly to uncertainty in modeled X_{CO_2} (Feng et al., 2019).

200   Here, we combine WRF-STILT back-trajectories with 4-D global mole fraction fields from simulations that were optimized using global *in-situ* measurements. From each receptor, 500 back-trajectories (simulating air parcels) are released and tracked backwards in time until the point at which they exit the WRF domain or for the duration of the simulation (10 days). At that coordinate (longitude, latitude, altitude, time) a global 4-D mole fraction field is sampled and that value is considered as the background value for that particle. Background values for all 500 particles are then averaged to calculate the estimated

205   background value for a given receptor. For background estimation, the WRF domain is subset to only include continental North America plus margins along the coast. These strategies minimize transport-related errors in the trajectories that inflate with increasing distance from the receptor and time of release. The background values for each receptor in a column are summed according to the pressure weighting function (eq. 2).

To assess errors due in global 4-D mole fraction fields used to estimate the background, we sample four different models that are informed by *in-situ* measurements and routinely updated. These include two versions of CarbonTracker (CT2016 and CT2019B; Peters et al., 2007; Jacobson et al., 2020) from NOAA's Global Monitoring Laboratory (GML), the Copernicus Atmosphere Monitoring Service reanalysis (CAMS; Chevallier et al., 2019) produced by the European Centre for Medium-Range Weather Forecasts (ECMWF), and the Jena CarboScope model from the Max Planck Institüt for Biogeochemistry (Rödenbeck et al., 2020). We evaluate each model against all designated assimilable CO_2 data from NOAA GML's GlobalView Plus version 6.0 data product (Table 1 Schuldt et al., 2020). Assimilable data include assimilated as well as withheld data. Withheld data are qualitatively equivalent to assimilated data (i.e., they pass the same quality flags) but are excluded and used to evaluate model results in CarbonTracker (A.R. Jacobson, pers. comm.). Here, over 150,000 ground, tall-tower and aircraft *in-situ* observations spanning 2014-15 over North America and the eastern North Pacific Ocean are used. Comparisons with these observations are provided for all assimilable observations, and assimilable observations between $4 - 8\,[km]$.

Table 1. Global CO_2 4D mole fraction fields used in this study. Comparisons with GML's GlobalView Plus version 6.0 data product are also presented. These comparisons are provided for all assimilable observations, and all assimilable observations between $4 - 8\,[km]$.

Model	Version	Resolution	Comparison with GV+ 6.0 obs [ppm]	
			all altitudes	4 to 8 $[km]$
CarbonTracker	CT2016	$3° \times 2° \times 3\,hrly$	0.49 ± 0.02	0.02 ± 0.03
CarbonTracker	CT2019B	$3° \times 2° \times 3\,hrly$	0.30 ± 0.01	0.05 ± 0.03
CAMS	v18r3 (2019)	$1.9° \times 3.75° \times 3\,hrly$	-0.73 ± 0.01	-0.18 ± 0.03
CarboScope	v4.3 (2019)	$6° \times 4° \times 6\,hrly$	0.60 ± 0.02	0.06 ± 0.03

2.5 Surface fluxes of CO_2: s

We sample optimized and imposed flux fields from regional and global inverse models. Net non-fire terrestrial ecosystem exchange (i.e., CO_2 fluxes from photosynthesis and respiration from autotrophic and heterotrophic sources or s_{bio}) are from NOAA's CarbonTracker-Lagrange (Hu et al., 2019). Briefly, CarbonTracker-Lagrange is a regional atmospheric inverse model in which biospheric fluxes for North America are optimized using surface-sensitivity arrays from high resolution WRF-STILT simulations and North American measurements of CO_2 from GlobalView+ v2.1 (Cooperative Global Atmospheric Data Integration Project, 2016), which is composed largely of data from NOAA's Global Greenhouse Gas Reference Network and from Environment and Climate Change Canada. Observations include flask-air measurements from near-surface and aircraft and quasi-continuous *in-situ* measurements primarily made on towers. The inversions were run with three different prior estimates of s_{bio}. These included two versions of the Carnegie-Ames Stanford Approach (CASA; Potter et al., 1993) biogeochemical model runs (CASA GFED-CMS and CASA GFEDv4.1) and the Combined Simple Biosphere/Carnegie-Ames-Stanford Approach terrestrial carbon cycle model (SiBCASA; Schaefer et al., 2008). Prior error covariance parameters were derived from

maximum likelihood estimation (MLE) with fixed correlation scales of $1000\,[km]$ and $7[days]$ and also for optimized correlation scales, for each model runs, resulting in six different posterior estimates of s_{bio}. Non-biospheric fluxes include imposed biomass burning (s_{bmb}) and fossil fuel (s_{ff}) fluxes, and optimized ocean fluxes (s_{ocn}) from CT2016. We use the mean of two

235   fossil fuel emission products ("Miller" and "ODIAC" datasets) and fire emission products ("GFED4.1s" and "GFED-CMS") used in CT2016. All fluxes are $1° \times 1°$ spatial and 3 hourly temporal resolution.

3   Results and discussion

3.1   Comparing simulated and satellite retrievals

For all retrievals selected over the spatiotemporal domain of this study, the impact of the OCO-2 bias correction is $2.01\,\pm$

240    $0.87\,[ppm]$, and the mean difference between seasons is $0.5\,[ppm]$ (1.76 in winter and spring, and $2.31\,[ppm]$ in summer; blue distributions in Fig. 3). Across seasons, the difference in residuals between $X_{\mathrm{CO_2}}^{ret,bc}$ and $X_{\mathrm{CO_2}}^{sim}$ is significantly lower than that between $X_{\mathrm{CO_2}}^{sim}$ and $X_{\mathrm{CO_2}}^{ret}$: $\mu_{sim-ret} = 2.23 \pm 1.36\,[ppm]$, whereas $\mu_{ret,bc-sim} = -0.22 \pm 1.91\,[ppm]$, i.e., the OCO-2 bias correction brings the distribution of OCO-2 $X_{\mathrm{CO_2}}$ substantially closer to the *in-situ* data-constrained synthetic columns ($X_{\mathrm{CO_2}}^{sim}$), as expected. Residuals are lowest in the Northern Hemisphere summer months of June, July and August

245   ($\mu_{ret,bc-sim} = 0.2 \pm 1.36\,[ppm]$; Fig. 3d) and highest in the winter and spring ($\mu_{ret,bc-sim} = -0.61\,[ppm]$; Fig. 3a). Apart from the summer, mean $X_{\mathrm{CO_2}}^{ret,bc}$ over North America is lower than $X_{\mathrm{CO_2}}^{sim}$.

3.2   Spatial patterns

To examine spatial patterns of simulated and retrieved soundings we first sort retrievals in $2° \times 2°$ bins and then average all retrievals (and simulations) in each bin for each season. The spatial extent of OCO-2 soundings varies seasonally (Fig. 4a,e,i,m).

250   The northern extent of valid retrievals follows the solar declination, as the OCO-2 spectrometer is unable to retrieve a signal over land that is dark or blanketed by snow. Consequently, between September and March, there are few soundings north of the U.S.- Canada border ($\sim 49°$N). Conversely, all of North America is observable between March and August.

Across seasons, $X_{\mathrm{CO_2}}^{sim}$ and $X_{\mathrm{CO_2}}^{ret,bc}$ exhibit broadly similar spatial patterns (Fig. 4a-n). However, residuals between the two reveal that $X_{\mathrm{CO_2}}^{ret,bc}$ is usually lower than $X_{\mathrm{CO_2}}^{sim}$, except in the summer, when a majority of retrievals in the eastern half of the

255   continent (right of the dotted lines in Fig. 4o) are higher than the simulations. Such coherent spatial differences are not evident when examining the mean bias over the continent (Fig. 3). Importantly, the magnitude of this difference is similar to that of the recent flux signals in the total column (Fig. 4d, h, l, p). For e.g., the mean residuals in the northeast quadrant during the summer (Fig. 4o) are $0.79 \pm 1.63\,[ppm]$, significantly higher than that for the entire domain ($0.09 \pm 1.38\,[ppm]$) and $\sim 45\%$ of the impact of recent surface flux on $X_{\mathrm{CO_2}}$, i.e., $\Delta_{CO_2}^{flux}$.
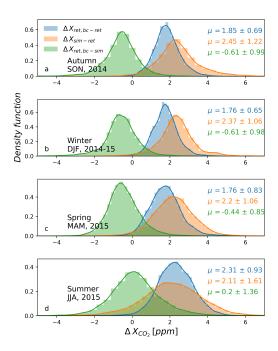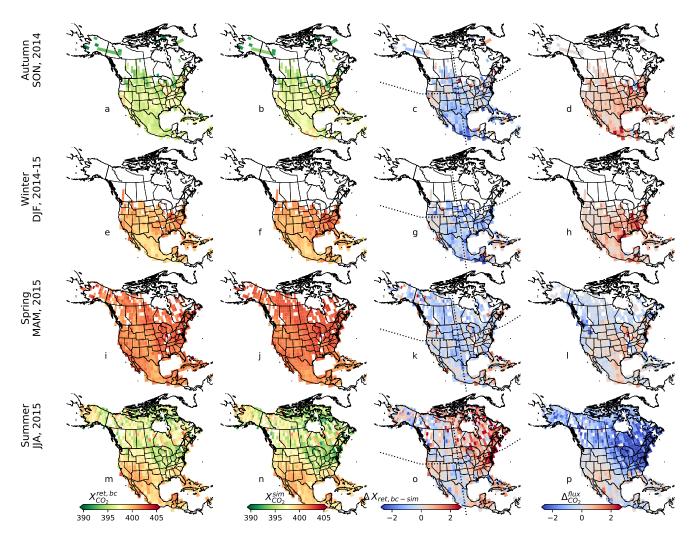
Figure 3. Kernel density distributions for residuals between simulated and satellite retrievals, grouped seasonally. Blue distributions show the impact of the OCO-2 bias correction on Land-Nadir retrievals. The orange and green curves show the difference between simulated retrievals and retrievals before and after bias correction respectively. Printed numbers report the mean and standard deviation of residuals. Uncertainties in $X_{\mathrm{CO_2}}^{sim}$ are discussed later in sec. 3.3.

3.3   Examining bias and uncertainty in $X_{\mathrm{CO_2}}^{sim}$

To establish whether differences between $X_{\mathrm{CO_2}}^{ret,bc}$ and $X_{\mathrm{CO_2}}^{sim}$ presented above (Figs. 3, 4) are due to residual biases in the former, we characterize systemic errors as well errors arising from unresolved variability in model fields used to construct $X_{\mathrm{CO_2}}^{sim}$. Cross-model standard deviations of four background models and $\Delta_{\mathrm{CO_2}}^{flux}$ from six biospheric flux ensembles on $X_{\mathrm{CO_2}}^{sim}$ is shown in Fig. 5. Cross model standard deviation in background fields is highest in the northwest during the summer ($0.36\ [ppm]$) but usually less than $0.3\ [ppm]$. Over the entire spatio-temporal domain of the study the standard deviation in estimates of $\Delta_{\mathrm{CO_2}}^{flux}$ and $X_{\mathrm{CO_2}}^{bkg}$ is $0.26 \pm 0.14\ [ppm]$ and $0.28 \pm 0.15\ [ppm]$ respectively. Model spread in $\Delta_{\mathrm{CO_2}}^{flux}$ is largest along the pacific coast of Mexico, a region that is relatively less well-constrained by the *in-situ* network. The standard deviation in $\Delta_{\mathrm{CO_2}}^{flux}$ is highest in the southeast quadrant in the summer ($0.32\ [ppm]$), but usually between 0.1 and $0.3\ [ppm]$. Uncertainty from model spread in flux and background is propagated in comparisons of $X_{\mathrm{CO_2}}^{sim}$ and $X_{\mathrm{CO_2}}^{ret,bc}$ presented earlier (Fig. 3).

Systematic error or bias in $X_{\mathrm{CO_2}}^{sim}$ can arise from errors in the estimation of background and surface flux, both of which are linked by an atmospheric transport model (Fig. 1). We use the same transport model used by Hu et al. (2019) to generate source-receptor relationships and background (secs. 2.3 and 2.4). Accuracy of the six-member ensemble of fluxes we use is also dependent upon the accuracy of WRF-STILT used in Hu et al. (2019). Thus, potential biases in WRF-STILT form a common
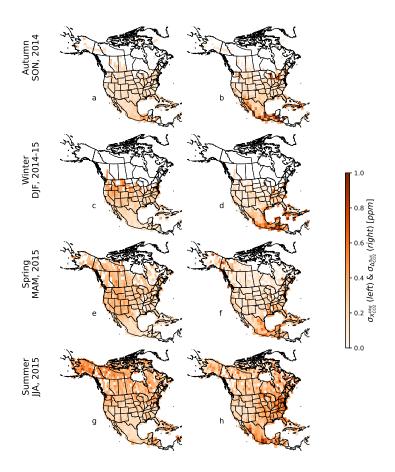
Figure 4. Spatial patterns of $X_{CO_2}^{ret,bc}$ (a, e, i, m), $X_{CO_2}^{sim}$ (b, f, j, n), $\Delta X_{sim-ret,bc}$ (c, g, k, o), and impact of recent surface flux ($\Delta_{CO_2}^{flux}$) on the $X_{CO_2}^{sim}$ (d, h, l, p) for soundings grouped seasonally and plotted on a $2° \times 2°$ grid. Units for all maps $[ppm]$. Dotted lines in c, g, k, o r are drawn along 40°N and 100°W.

thread for error propagation. The combined accuracy of fluxes and transport is evaluated by examining aircraft vertical profiles

275 of CO_2 collected under NOAA GML's aircraft program (Sweeney et al., 2015, https://www.esrl.noaa.gov/gmd/ccgg/aircraft/) *not* assimilated by Hu et al. (2019). We simulate all independent aircraft observations over North America for 2007-2015 (the entire spatiotemporal range of Hu et al., 2019) using existing WRF-STILT source-receptor relationships. To ensure consistency with Hu et al. (2019), we perform this evaluation with the same background conditions as in that study (i.e., CT2016). Aircraft profiles are sorted in $1\,[km]$ altitude bins from the surface to $8\,[km]\,a.s.l.$ and separated by season. Aircraft vertical profiles

280 of CO_2 (after removing the influence of background) as well as surface fluxes propagated with WRF-STILT show net release

Figure 5. Cross model standard deviations flux impact (a, c, e, g) and background models (b, d, f, h). Six biospheric flux ensembles and four model fields for background are used in this study.

of CO_2 in non-summer months and net uptake from photosynthesis depleting near-surface CO_2 during the summer (green triangles and pink hexagons in Fig. 6a, c, e, g respectively). The difference between independent, unassimilated observations and simulations show that bias at any given altitude level for any season is usually less than $0.5\,[ppm]$ (Fig. 6b, e, h, j). Bias is also usually largest near the surface (except in spring). The pressure-weighted partial column (from the surface to $8\,[km]$ a.s.l.)

285 mean bias ($\mu_{sim-obs}$) ranges from -0.12 in autumn to $0.18\,[ppm]$ in the spring and is comparable to the typical measurement uncertainty within the *in-situ* Global Greenhouse Gasses Research Network of $\sim\ \ 0.15$ [ppm] as derived from long term comparisons of differences between different within-network sampling and analysis approaches for CO_2 (e.g., Andrews et al., 2014; Lan et al., 2017; Sweeney et al., 2015). Low partial column bias relative to independent vertical profile CO_2 data show that errors in WRF-STLT transport contribute very minimally to bias in $X_{CO_2}^{sim}$.

290 To examine potential systematic errors in the highest part of the column, (above $8\,[km]$ i.e., the upper troposphere and the stratosphere), we compare 4-D model fields used in this study with CO_2 profiles collected by NOAA GML's AirCore program
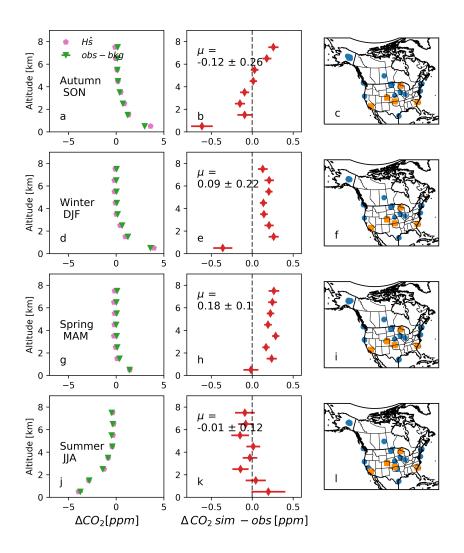
Figure 6. Simulated and observed vertical profiles from independent *in-situ* aircraft observations collected over 2007-2015 (a, c, e, g), showing simulated enhancements or depletion in CO_2 as a result of surface flux (pink hexagons). Additionally, the difference between observations and CT2016 background is plotted (green triangles). We report the vertically resolved and *pressure weighted* bias (mean and standard deviation) between simulations and observations (b, d, f, h). Finally, a map shows the location of aircraft profiles (blue circles-i) The size of each data point indicates relative number of samples. Additionally, AirCore profile locations are also shown (orange squares-i). AirCore data are used to evaluate biases in boundary conditions in the upper 350 [hPa] of the column and are presented in table 2.

(Karion et al., 2010, data version "v20200210"). There is a considerably larger spread in models' ability to replicate AirCore observations (Table 2) than surface and aircraft observations (Table 1 and Fig. 6). Bias between model and observations varies seasonally, is highest in the spring and lowest in the summer. However, this region forms the upper ~ 350 [hPa] of the column. This has two implications. First, the contribution to total column bias reduces by $\sim 65\%$. Second, the ACOS convolution equation (eq. 1) requires modeled estimates of X_{CO_2} be appropriately weighted with the averaging kernel (a_i). a_i determines the balance between information obtained by the retrieval and that contained in the OCO-2 prior ($\chi_{CO_2}^{pri}$), and tends to decrease from ~ 1 near the surface to < 0.5 in the upper third of the column. Thus $\sim 50\%$ of the error in the highest 350 [hPa] of the simulated column is due to errors in $\chi_{CO_2}^{pri}$. Consequently, the total contribution of model bias presented in Table 2 contributes to only $\sim 50\%$ of the bias in $X_{CO_2}^{sim}$ in the uppermost third of the column. The other source of error above 8 [km] is the error in $\chi_{CO_2}^{pri}$, but this information is currently unavailable in the OCO-2 *v10* lite files and is thus ignored in our error analysis. However, errors in $\chi_{CO_2}^{pri}$ are identical for $X_{CO_2}^{sim}$ and $X_{CO_2}^{ret,bc}$ and do not affect comparisons between the two.

Table 2. Systematic bias between global 4D CO_2 fields and AirCore profiles above 8 [km]. Across-model mean and standard deviation is weighted with the pressure weighting function and OCO-2 averaging kernel. All values in [ppm]. Location of AirCore profiles is shown as orange squares in Fig. 6i.

Season	CT 2016	CT 2019B	CAMS	CarboScope	$\mu_{models} \pm \sigma_{models}$
Autumn	0.59 ± 0.02	0.77 ± 0.01	0.27 ± 0.01	0.95 ± 0.02	0.11 ± 0.04
Winter	0.57 ± 0.01	0.74 ± 0.01	0.34 ± 0.01	1.99 ± 0.02	0.16 ± 0.19
Spring	$--$	1.40 ± 0.03	0.76 ± 0.03	3.31 ± 0.07	0.32 ± 0.19
Summer	0.4 ± 0.04	0.45 ± 0.02	-0.11 ± 0.02	0.73 ± 0.03	0.06 ± 0.05

Combined with the standard deviation across 24 flux-background ensemble members that comprise $X_{CO_2}^{sim}$, comparisons with independent unassimilated aircraft (Fig. 6) and AirCore profiles (Table 2) allow us to comprehensively assess uncertainties associated with $X_{CO_2}^{sim}$. We estimate the combined uncertainty from surface flux, background estimation and transport as:

$$\sigma_{X_{CO2}^{sim}} = \mu_{model-aircraft} + \mu_{model-AirCore} \pm \sqrt{(\sigma_{model-aircraft})^2 + (\sigma_{model-AirCore})^2 + (\sigma_{flux+bkg\ ensembles})^2} \quad (5)$$

where

$$\sigma_{flux+bkg\ ensembles} = \sqrt{\sigma_{flux\ ensembles}^2 + \sigma_{bkg\ ensembles}^2 + 2\sigma_{flux,bkg}} \quad (6)$$

The first two terms in eq. 5 represent the *pressure-weighted* mean partial column bias between modeled and observed CO_2 vertical profiles from aircraft (Fig. 6) and aircore (Table 2) respectively. The sum of these two terms provides an estimate of bias or systematic error. The third term in eq. 5 represents unresolved variability.

Table 3. Total uncertainty estimates for $X_{CO_2}^{sim}$, the mean difference between $X_{CO_2}^{sim}$ and $X_{CO_2}^{ret,bc}$, and bias in $X_{CO_2}^{ret,bc}$. Bias is obtained as the difference between the first two terms in the middle and left columns. All values in $[ppm]$. The number on the right in the third column indicates the spatial variability in $X_{CO_2}^{ret,bc}$ bias. Finally we also present the same quantity for the previous version of OCO-2 retrievals, the *v9* data product. Note, for *v9* only land-nadir retrievals are analysed.

Season	$\sigma_{X_{CO2}^{sim}}$	$\Delta X_{ret,bc-sim}$	Bias in $X_{CO_2}^{ret,bc}$	Bias in $X_{CO_2}^{ret,bc}$ *v9-LN*
Autumn	-0.01 ± 0.31	-0.61 ± 0.99	-0.62 ± 0.99	-0.88 ± 1.00
Winter	0.25 ± 0.35	-0.61 ± 0.98	-0.36 ± 0.98	-0.76 ± 1.10
Spring	0.50 ± 0.31	-0.44 ± 0.85	0.06 ± 0.85	0.07 ± 0.99
Summer	0.05 ± 0.40	0.20 ± 1.36	0.25 ± 1.36	0.14 ± 1.38

We find that unresolved variability due to model spread in $X_{CO_2}^{sim}$ is $\sim 0.35\ [ppm]$ (second term under $\sigma_{X_{CO_2}^{sim}}$ in Table 3), similar across seasons, and significantly lower than the uncertainty of $X_{CO_2}^{ret,bc}$ as reported in the OCO-2 *v10 lite* files (~ 0.6 [ppm]). Systematic error or bias in $X_{CO_2}^{sim}$ (first term under $\sigma_{X_{CO2}^{sim}}$ in Table 3) shows significant variability across seasons.

315 Comparing this to $\Delta X_{ret,bc-sim}$ allows an estimation of mean bias in $X_{CO_2}^{ret,bc}$ over North America (Table 3). We find that $X_{CO_2}^{ret,bc}$ bias ranges from $-0.62\ [ppm]$ in autumn to $0.14\ [ppm]$ in summer. This indicates that $\Delta X_{ret,bc-sim}$ in autumn (Fig. 3a and Fig. 4c) is entirely due to a residual bias in $X_{CO_2}^{ret,bc}$ but almost entirely due to bias in $\sigma_{X_{CO2}^{sim}}$ in the spring (Fig. 3c and Fig. 4k). During summer the mean bias in $X_{CO_2}^{sim}$ is $0.05\ [ppm]$, and consequently the mean bias in $X_{CO_2}^{ret,bc}$ is $0.25\ [ppm]$. However, the mean conceals larger regional differences. In the northeast quadrant for instance, $\Delta X_{ret,bc-sim}$ (Fig. 4o) of

320 $0.79\ [ppm]$ translates to a high bias $0.84\ [ppm]$ during the summer. Finally, we find that the OCO-2 *v10* bias correction shows an improvement over the *v9* bias correction, particularly in the winter.

3.4 Evaluating the OCO-2 bias correction

Bias in OCO-2 *v10* X_{CO_2} is a combination of footprint bias (8 coincident across track retrievals; C_f) and feature biases (related to surface or atmospheric parameters, e.g., aerosol optical depth; C_p). Finally, a global scaling factor (C_0) obtained

325 from comparisons with TCCON retrievals, is used to empirically link retrievals to the WMO scale.

To examine residual feature biases, we perform simple linear regressions between parameters used in the OCO-2 *v10* bias correction with $\Delta X_{ret,bc-sim}$. These parameters are $\Delta P_{frac}\ [ppm]$, which accounts for fractional change in X_{CO_2} due to difference in prior and retrieved surface pressure (Kiel et al., 2019), $CO_2\text{-}grad\ del$, defined as the difference of the difference between retrieved and prior CO_2 at the surface and at 0.7 times the surface pressure, dws, which is the total retrieved optical

330 depth associated with aerosols from dust, water cloud and aerosol and aod_{fine}, the aerosol optical depth from sulfate and organic carbon (O'Dell et al., 2018; Osterman et al., 2020). Additionally, we perform simple linear regressions with altitude and surface albedo. All parameters are available in the OCO-2 *v10 lite* files. We find no significant correlations observed

between $\Delta\Delta X_{ret,bc-sim}$ and any parameters suggesting that there are no regional scale parametric biases over North America for our study period that are not already removed by the OCO-2 global bias correction.

335   We then evaluate the OCO-2 *v10* global scaling by obtaining scaling factors ($C_{0,sim}$) for North America. First, we 'de-link' $X_{CO_2}^{ret,bc}$ from TCCON by multiplying it with C_0. Then we invert the framework defined by O'Dell et al. (2018) and obtain $C_{0,sim}$ as the slope of a linear regression between $X_{CO_2}^{sim}$ and $X_{CO_2}^{ret,bc}$ that is forced through the origin, with associated uncertainties (York et al., 2004). $X_{CO_2}^{sim}$ uncertainty is characterized as the standard deviation of all background and flux ensemble members described in 2.4 and 2.5. We also propagate both systematic errors and residual errors due to unresolved

340   variability in $X_{CO_2}^{sim}$ (sec. 3). We use the reported uncertainty of each retrieval as uncertainty in $X_{CO_2}^{ret}$. $C_{0,sim}$ varies seasonally for 2014-15 and is also different from the static, global, multi-year number used for land-nadir retrievals currently (Table 4). To test the impact of this difference, we scale $X_{CO_2}^{ret,bc}$ with $C_{0,sim} - C_0$ for each season. The mean ΔX_{CO_2} [ppm] for all retrievals is presented in the third column in table 4, and indicates the magnitude by which $X_{CO_2}^{ret,bc}$ would have to change so as to be consistent with $X_{CO_2}^{sim}$., i.e. the *in-situ* network over North America. For e.g., if instead of the TCCON network, $X_{CO_2}^{sim}$ is

345   used to scale land-nadir OCO-2 *v10* soundings over North America, $X_{CO_2}^{ret,bc}$ would reduce by -0.61 [ppm] in autumn.
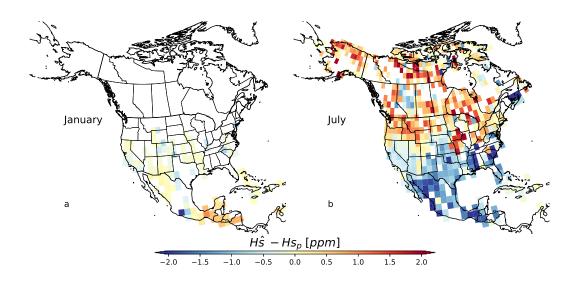
Table 4. Scaling factors for global bias obtained from $X_{CO_2}^{sim}$ ($C_{0,sim}$) and the global number used in the OCO-2 bias correction (C_0). $C_{0,sim}$ varies seasonally while C_0 is constant. The error in $C_{0,sim}$ is $< 1.0e^{-4}$ for all regressions. ΔX_{CO_2} is calculated by multiplying the difference between $C_{0,sim}$ and C_0 with the mean $X_{CO_2}^{ret,bc}$ for each season and indicates the magnitude by which $X_{CO_2}^{ret,bc}$ would have to adjust if $X_{CO_2}^{sim}$ is used in global scaling, instead of TCCON.

Season	$C_{0,sim}$	C_0	ΔX_{CO_2} [ppm]
Autumn	0.9943		-0.61
Winter	0.9950		-0.36
Spring	0.9960		0.06
Summer	0.9965		0.24
Annual	0.9960	0.9959	0.24

4   Implications for carbon flux estimation

The impact of recent surface flux on $X_{CO_2}^{sim}$ is small (e.g. right column in Fig. 4). The interquartile range of $\Delta_{CO_2}^{flux}$ over the entire spatiotemporal domain is less than 1 [ppm] implying that the imprint of recent surface flux on the total column is roughly half the magnitude of the OCO-2 bias correction (blue curves in Fig.3). Moreover, only around 2 % of simulations in

350   the summer (when surface fluxes are highest) are associated with absolute $\Delta_{CO_2}^{flux}$ magnitudes higher than 4 [ppm], indicating that recent surface flux rarely accounts for more than a ~ 1 % change in $X_{CO_2}^{sim}$. In autumn, $\Delta_{CO_2}^{flux}$ is of the same magnitude as bias in $X_{CO_2}^{ret,bc}$ (Table 3). OCO-2 retrievals in autumn 2014 are therefore unlikely to provide reliable estimates of North

Figure 7. Difference between prior and optimized biospheric flux from CarbonTracker Lagrange show small differences, when projected onto the total column [ppm].

American surface flux. During the summer, OCO-2 has a high bias of $0.25\,[ppm]$ over the continent, but this bias may be significantly larger in the eastern half of the domain (Fig. 4o). In the northeast quadrant for example, a potential bias of $0.84\,[ppm]$ constitutes ~ 47 % of the mean $\Delta_{CO_2}^{flux}$ of $-1.79\,[ppm]$. Considering that the vast majority of current inverse modeling or data assimilation systems used for CO_2 flux estimation are designed to correct errors in an *a priori* estimate, the effective signal is considerably smaller than what is shown here (right column in Fig. 4). In fact, when projected onto the total column, we find that the difference between a biospheric prior flux model (CASA-CMS) and flux optimized by the CT-Lagrange inversion system (using the same prior flux estimate; Hu et al., 2019) for January and July, 2015 are 0.15 ± 0.38 and $0.09 \pm 1.06\,[ppm]$ respectively. Continental scale aggregations mask regional differences (Fig. 7), but flux adjustment impacts on $X_{CO_2}^{sim}$ are usually indistinguishable from 0 in January and greater than $\pm 1\,[ppm]$ for less than a third of simulated retrievals in July, when biospheric uptake over North America is highest. Errors in terrestrial biosphere models of CO_2 flux translate to similarly small impacts on X_{CO_2}, posing questions on the utility of these data currently in evaluating terrestrial biosphere models.

5 Conclusions

In this study, we compare one year of $X_{CO_2}^{ret,bc}$ over North America from NASA's OCO-2 (*v10*; *land-nadir* and *glint* retrievals) satellite against synthetic columns that are constructed using a high-resolution regional model of atmospheric transport and

driven by fluxes and background that are optimally consistent with *in-situ* measurements of CO_2 dry air mole fraction, which are rigorously calibrated to the WMO CO_2 X2007 scale. Although X_{CO_2} from OCO-2 and from the posterior of *in-situ* data

370　inversions has been compared previously, and used in its bias correction (O'Dell et al., 2018; Kiel et al., 2019), this is the first such evaluation at the regional scale that uses high-resolution atmospheric transport. We use a suite of optimized non-fire net ecosystem exchange fluxes and background fields to assess under in $X_{CO_2}^{sim}$. Potential systematic errors in fluxes, transport, and background fields are evaluated by comparisons with vertical gradients of atmospheric CO_2 from independent aircraft and AirCore vertical profiles. $X_{CO_2}^{sim}$ is associated with errors arising from unresolved variability in model fields, and systematic

375　bias. The first of these results in an uncertainty of ~ 0.35 [ppm]. Bias or systematic error in $X_{CO_2}^{sim}$ is found to vary seasonally and ranges from -0.01 [ppm] in autumn to 0.50 [ppm] in the spring. Bias is highest in the upper \$ 350 [h Pa] of the column (Table 2), a region that is most poorly constrained by atmospheric measurements. However, the effect of this bias is relatively small in the total column comparisons.

　　Comparisons with $X_{CO_2}^{sim}$ show that the OCO-2 *v10* global bias correction greatly improves the quality of OCO-2 data over

380　North America (Fig. 3). However, generally good agreement between $X_{CO_2}^{ret,bc}$ and $X_{CO_2}^{sim}$ at the continental scale masks significant differences at regional scales and for some seasons (Fig. 4). Error analysis of the components of $X_{CO_2}^{sim}$ (i.e., transport, background, and flux) allows us to better characterize difference between simulations and retrievals. Differences in $\Delta X_{ret,bc-sim}$ are highest in autumn and indicative of a low bias in $X_{CO_2}^{ret,bc}$ of 0.62 [ppm] which is identical to the mean impact of recent surface flux (mean $\Delta_{CO_2}^{flux}$ over the continent is 0.64 [ppm]) in that season. In winter, a low bias in $X_{CO_2}^{ret,bc}$

385　of 0.36 [ppm] is roughly 50% of the mean $\Delta_{CO_2}^{flux}$ of 0.71 [ppm]. In summer we find spatially coherent regional patterns in $\Delta X_{ret,bc-sim}$. $\Delta X_{ret,bc-sim}$ is highest in the northeast quadrant of North America (Fig. 4o) at -0.81 [ppm], 50% of the mean expected ecosystem flux impact over this region. Since inverse models of CO_2 flux usually optimize a prior flux estimate, the surface flux signal (i.e., difference between prior and optimized flux) in X_{CO_2} is minuscule (Fig. 7), significantly smaller than the magnitude of the OCO-2 *v10* bias correction, and translates to extremely strenuous requirements on the quality of

390　space-based retrievals. The OCO-2 community has worked diligently to reduce uncertainty on satellite retrievals (e.g., O'Dell et al., 2012, 2018; Kiel et al., 2019; Wunch et al., 2017; Kulawik et al., 2019); bias in *v10* retrievals over North America has reduced in autumn and winter of 2014-15 compared to the *v9* data product (Table 3), but further improvement is necessary for both existing satellite datasets and planned missions that will provide this quantity in order to accurately constrain surface fluxes in a changing climate. Finally, we argue that a greatly expanded global reference network of calibrated *in-situ* vertical

395　profile measurements is necessary to reliably detect and correct systematic errors in satellite X_{CO_2}.

References

Alden, C. B., Miller, J. B., Gatti, L. V., Gloor, M. M., Guan, K., Michalak, A. M., van der Laan-Luijkx, I. T., Touma, D., Andrews, A., Basso, L. S., Correia, C. S., Domingues, L. G., Joiner, J., Krol, M. C., Lyapustin, A. I., Peters, W., Shiga, Y. P., Thoning, K., van der Velde, I. R., van Leeuwen, T. T., Yadav, V., and Diffenbaugh, N. S.: Regional atmospheric CO2 inversion reveals seasonal and geographic differences in Amazon net biome exchange, Global change biology, 22, 3427–3443, https://doi.org/10.1111/gcb.13305, 2016.

Andrews, A. E., Kofler, J. D., Trudeau, M. E., Williams, J. C., Neff, D. H., Masarie, K. A., Chao, D. Y., Kitzis, D. R., Novelli, P. C., Zhao, C. L., Dlugokencky, E. J., Lang, P. M., Crotwell, M. J., Fischer, M. L., Parker, M. J., Lee, J. T., Baumann, D. D., Desai, A. R., Stanier, C. O., De Wekker, S. F., Wolfe, D. E., Munger, J. W., and Tans, P. P.: CO2, CO, and CH4 measurements from tall towers in the NOAA earth system research laboratory's global greenhouse gas reference network: Instrumentation, uncertainty analysis, and recommendations for future high-accuracy greenhouse gas monitoring efforts, Atmospheric Measurement Techniques, 7, 647–687, https://doi.org/10.5194/amt-7-647-2014, 2014.

Arora, V. K., Katavouta, A., Williams, R. G., Jones, C. D., Brovkin, V., Friedlingstein, P., Schwinger, J., Bopp, L., Boucher, O., Cadule, P., Chamberlain, M. A., Christian, J. R., Delire, C., Fisher, R. A., Hajima, T., Ilyina, T., Joetzjer, E., Kawamiya, M., Koven, C. D., Krasting, J. P., Law, R. M., Lawrence, D. M., Lenton, A., Lindsay, K., Pongratz, J., Raddatz, T., Séférian, R., Tachiiri, K., Tjiputra, J. F., Wiltshire, A., Wu, T., and Ziehn, T.: Carbon–concentration and carbon–climate feedbacks in CMIP6 models and their comparison to CMIP5 models, Biogeosciences, 17, 4173–4222, https://doi.org/10.5194/bg-17-4173-2020, https://bg.copernicus.org/articles/17/4173/2020/, 2020.

Ballantyne, A. P., Alden, C. B., Miller, J. B., Trans, P. P., and White, J. W.: Increase in observed net carbon dioxide uptake by land and oceans during the pst 50 years, Nature, 488, 70–73, https://doi.org/10.1038/nature11299, http://dx.doi.org/10.1038/nature11299, 2012.

Basu, S., Guerlet, S., Butz, A., Houweling, S., Hasekamp, O., Aben, I., Krummel, P., Steele, P., Langenfelds, R., Torn, M., Biraud, S., Stephens, B., Andrews, A., and Worthy, D.: Global CO2 fluxes estimated from GOSAT retrievals of total column CO2, Atmospheric Chemistry and Physics, 13, 8695–8717, https://doi.org/10.5194/acp-13-8695-2013, 2013.

Basu, S., Baker, D. F., Chevallier, F., Patra, P. K., Liu, J., and Miller, J. B.: The impact of transport model differences on CO2 surface flux estimates from OCO-2 retrievals of column average CO2, Atmospheric Chemistry and Physics, 18, 7189–7215, https://doi.org/10.5194/acp-18-7189-2018, 2018.

Byrne, B., Liu, J., Lee, M., Baker, I., Bowman, K. W., Deutscher, N. M., Feist, D. G., Griffith, D. W. T., Iraci, L. T., Kiel, M., Kimball, J. S., Miller, C. E., Morino, I., Parazoo, N. C., Petri, C., Roehl, C. M., Sha, M. K., Strong, K., Velazco, V. A., Wennberg, P. O., and Wunch, D.: Improved Constraints on Northern Extratropical CO 2 Fluxes Obtained by Combining Surface-Based and Space-Based Atmospheric CO 2 Measurements, Journal of Geophysical Research: Atmospheres, 125, https://doi.org/10.1029/2019JD032029, https://onlinelibrary.wiley.com/doi/abs/10.1029/2019JD032029, 2020.

Chevallier, F., Palmer, P. I., Feng, L., Boesch, H., O'Dell, C. W., and Bousquet, P.: Toward robust and consistent regional CO 2 flux estimates from in situ and spaceborne measurements of atmospheric CO 2, Geophysical Research Letters, 41, 1065–1070, https://doi.org/10.1002/2013GL058772, http://doi.wiley.com/10.1002/2013GL058772, 2014.

Chevallier, F., Remaud, M., O'Dell, C. W., Baker, D., Peylin, P., and Cozic, A.: Objective evaluation of surface- and satellite-driven carbon dioxide atmospheric inversions, Atmospheric Chemistry and Physics, 19, 14 233–14 251, https://doi.org/10.5194/acp-19-14233-2019, 2019.

Connor, B. J., Boesch, H., Toon, G., Sen, B., Miller, C., and Crisp, D.: Orbiting Carbon Observatory: Inverse method and prospective error analysis, Journal of Geophysical Research Atmospheres, 113, 1–14, https://doi.org/10.1029/2006JD008336, 2008.

Cooperative Global Atmospheric Data Integration Project: Multi-laboratory compilation of atmospheric carbon dioxide data for the period 1957-2015; obspack_co2_1_GLOBALVIEWplus_v2.1_2016-09-02, https://doi.org/10.15138/G3059Z, http://www.esrl.noaa.gov/gmd/ccgg/obspack/data.php?id=obspack_co2_1_GLOBALVIEWplus_v2.1_2016-09-02, 2016.

445

Corbin, K. D., Denning, A. S., Lu, L., Wang, J.-W., and Baker, I. T.: Possible representation errors in inversions of satellite CO 2 retrievals, Journal of Geophysical Research, 113, D02 301, https://doi.org/10.1029/2007JD008716, http://doi.wiley.com/10.1002/2013JD020175http://doi.wiley.com/10.1029/2007JD008716, 2008.

Crowell, S., Baker, D., Schuh, A., Basu, S., Jacobson, A. R., Chevallier, F., Liu, J., Deng, F., Feng, L., McKain, K., Chatterjee, A., Miller, J. B., Stephens, B. B., Eldering, A., Crisp, D., Schimel, D., Nassar, R., O'Dell, C. W., Oda, T., Sweeney, C., Palmer, P. I., and Jones, D. B.: The 2015-2016 carbon cycle as seen from OCO-2 and the global in situ network, Atmospheric Chemistry and Physics, 19, 9797–9831, https://doi.org/10.5194/acp-19-9797-2019, 2019.

450

DeVries, T., Le Quéré, C., Andrews, O., Berthet, S., Hauck, J., Ilyina, T., Landschützer, P., Lenton, A., Lima, I. D., Nowicki, M., Schwinger, J., and Séférian, R.: Decadal trends in the ocean carbon sink, Proceedings of the National Academy of Sciences of the United States of America, 116, 11 646–11 651, https://doi.org/10.1073/pnas.1900371116, 2019.

455

Eldering, A., O'Dell, C. W., Wennberg, P. O., Crisp, D., Gunson, M. R., Viatte, C., Avis, C., Braverman, A., Castano, R., Chang, A., Chapsky, L., Cheng, C., Connor, B., Dang, L., Doran, G., Fisher, B., Frankenberg, C., Fu, D., Granat, R., Hobbs, J., Lee, R. A., Mandrake, L., McDuffie, J., Miller, C. E., Myers, V., Natraj, V., O'Brien, D., Osterman, G. B., Oyafuso, F., Payne, V. H., Pollock, H. R., Polonsky, I., Roehl, C. M., Rosenberg, R., Schwandner, F., Smyth, M., Tang, V., Taylor, T. E., To, C., Wunch, D., and Yoshimizu, J.: The Orbiting Carbon Observatory-2: First 18 months of science data products, Atmospheric Measurement Techniques, 10, 549–563, https://doi.org/10.5194/amt-10-549-2017, 2017.

460

Feng, S., Lauvaux, T., Davis, K. J., Keller, K., Zhou, Y., Williams, C., Schuh, A. E., Liu, J., and Baker, I.: Seasonal Characteristics of Model Uncertainties From Biogenic Fluxes, Transport, and Large-Scale Boundary Inflow in Atmospheric CO2 Simulations Over North America, Journal of Geophysical Research: Atmospheres, 124, 14 325–14 346, https://doi.org/10.1029/2019JD031165, 2019.

465

Fischer, M. L., Parazoo, N., Brophy, K., Cui, X., Jeong, S., Liu, J., Keeling, R., Taylor, T. E., Gurney, K., Oda, T., and Graven, H.: Simulating estimation of California fossil fuel and biosphere carbon dioxide exchanges combining in situ tower and satellite column observations, Journal of Geophysical Research, 122, 3653–3671, https://doi.org/10.1002/2016JD025617, 2017.

Gourdji, S. M., Mueller, K. L., Yadav, V., Huntzinger, D. N., Andrews, A. E., Trudeau, M., Petron, G., Nehrkorn, T., Eluszkiewicz, J., Henderson, J., Wen, D., Lin, J., Fischer, M., Sweeney, C., and Michalak, A. M.: North American CO2 exchange: Inter-comparison of modeled estimates with results from a fine-scale atmospheric inversion, Biogeosciences, 9, 457–475, https://doi.org/10.5194/bg-9-457-2012, 2012.

470

Gurney, K. R., Law, R. M., Denning, A. S., Rayner, P. J., Baker, D., Bousquet, P., Bruhwiler, L., Chen, Y. H., Ciais, P., Fan, S., Fung, I. Y., Gloor, M., Heimann, M., Higuchi, K., John, J., Maki, T., Maksyutov, S., Masarie, K., Peylin, P., Prather, M., Pak, B. C., Randerson, J., Sarmiento, J., Taguchi, S., Takahashi, T., and Yuen, C. W.: Towards robust regional estimates of annual mean {CO}_2 sources and sinks, Nature, 415, 626–630, 2002.

475

Hall, B. D., Crotwell, A. M., Kitzis, D. R., Mefford, T., Miller, B. R., Schibig, M. F., and Tans, P. P.: Revision of the WMO/GAW \chem{CO_2} Calibration Scale, Atmospheric Measurement Techniques Discussions, 2020, 1–33, https://doi.org/10.5194/amt-2020-408, https://amt.copernicus.org/preprints/amt-2020-408/, 2020.

Heimann, M. and Reichstein, M.: Terrestrial ecosystem carbon dynamics and climate feedbacks, Nature, 451, 289–292, https://doi.org/10.1038/nature06591, http://www.nature.com/articles/nature06591, 2008.

480

Houweling, S., Breon, F.-M., Aben, I., Rödenbeck, C., Gloor, M., Heimann, M., and Ciais, P.: Inverse modeling of CO<sub>2</sub> sources and sinks using satellite data: A synthetic inter-comparison of measurement techniques and their performance as a function of space and time, Atmospheric Chemistry and Physics Discussions, 3, 5237–5274, https://doi.org/10.5194/acpd-3-5237-2003, 2003.

485 Hu, L., Andrews, A. E., Thoning, K. W., Sweeney, C., Miller, J. B., Michalak, A. M., Dlugokencky, E., Tans, P. P., Shiga, Y. P., Mountain, M., Nehrkorn, T., Montzka, S. A., McKain, K., Kofler, J., Trudeau, M., Michel, S. E., Biraud, S. C., Fischer, M. L., Worthy, D. E., Vaughn, B. H., White, J. W., Yadav, V., Basu, S., and Van Der Velde, I. R.: Enhanced North American carbon uptake associated with El Niño, Science Advances, 5, https://doi.org/10.1126/sciadv.aaw0076, 2019.

Jacobson, A. R., Schuldt, K. N., Miller, J. B., Oda, T., Tans, P., Arlyn Andrews, Mund, J., Ott, L., Collatz, G. J., Aalto, T., Afshar, S.,
490 Aikin, K., Aoki, S., Apadula, F., Baier, B., Bergamaschi, P., Beyersdorf, A., Biraud, S. C., Bollenbacher, A., Bowling, D., Brailsford, G., Abshire, J. B., Chen, G., Huilin Chen, Lukasz Chmura, Sites Climadat, Colomb, A., Conil, S., Cox, A., Cristofanelli, P., Cuevas, E., Curcoll, R., Sloop, C. D., Davis, K., Wekker, S. D., Delmotte, M., DiGangi, J. P., Dlugokencky, E., Ehleringer, J., Elkins, J. W., Emmenegger, L., Fischer, M. L., Forster, G., Frumau, A., Galkowski, M., Gatti, L. V., Gloor, E., Griffis, T., Hammer, S., Haszpra, L., Hatakka, J., Heliasz, M., Hensen, A., Hermanssen, O., Hintsa, E., Holst, J., Jaffe, D., Karion, A., Kawa, S. R., Keeling, R., Keronen,
495 P., Kolari, P., Kominkova, K., Kort, E., Krummel, P., Kubistin, D., Labuschagne, C., Langenfelds, R., Laurent, O., Laurila, T., Lauvaux, T., Law, B., Lee, J., Lehner, I., Leuenberger, M., Levin, I., Levula, J., Lin, J., Lindauer, M., Loh, Z., Lopez, M., Luijkx, I. T., Myhre, C. L., Machida, T., Mammarella, I., Manca, G., Manning, A., Manning, A., Marek, M. V., Marklund, P., Martin, M. Y., Matsueda, H., McKain, K., Meijer, H., Meinhardt, F., Miles, N., Miller, C. E., Mölder, M., Montzka, S., Moore, F., Josep-Anton Morgui, Morimoto, S., Munger, B., Jaroslaw Necki, Newman, S., Nichol, S., Niwa, Y., O'Doherty, S., Mikaell Ottosson-Löfvenius, Paplawsky, B., Peischl,
500 J., Peltola, O., Jean-Marc Pichon, Piper, S., Plass-Dölmer, C., Ramonet, M., Reyes-Sanchez, E., Richardson, S., Riris, H., Ryerson, T., Saito, K., Sargent, M., Sasakawa, M., Sawa, Y., Say, D., Scheeren, B., Schmidt, M., Schmidt, A., Schumacher, M., Shepson, P., Shook, M., Stanley, K., Steinbacher, M., Stephens, B., Sweeney, C., Thoning, K., Torn, M., Turnbull, J., Tørseth, K., Bulk, P. V. D., Dinther, D. V., Vermeulen, A., Viner, B., Vitkova, G., Walker, S., Weyrauch, D., Wofsy, S., Worthy, D., Dickon Young, and Miroslaw Zimnoch: CarbonTracker CT2019B, https://doi.org/10.25925/20201008, https://www.esrl.noaa.gov/gmd/ccgg/carbontracker/CT2019B/, 2020.

505 Karion, A., Sweeney, C., Tans, P., and Newberger, T.: AirCore: An innovative atmospheric sampling system, Journal of Atmospheric and Oceanic Technology, 27, 1839–1853, https://doi.org/10.1175/2010JTECHA1448.1, 2010.

Keeling, R. F., Graven, H. D., Welp, L. R., Resplandy, L., Bi, J., Piper, S. C., Sun, Y., Bollenbacher, A., and Meijer, H. A. J.: Atmospheric evidence for a global secular increase in carbon isotopic discrimination of land photosynthesis, Proceedings of the National Academy of Sciences, p. 201619240, https://doi.org/10.1073/pnas.1619240114, http://www.pnas.org/lookup/doi/10.1073/pnas.1619240114, 2017.

510 Kiel, M., O'Dell, C. W., Fisher, B., Eldering, A., Nassar, R., MacDonald, C. G., and Wennberg, P. O.: How bias correction goes wrong: Measurement of XCO2 affected by erroneous surface pressure estimates, Atmospheric Measurement Techniques, 12, 2241–2259, https://doi.org/10.5194/amt-12-2241-2019, 2019.

Kulawik, S. S., O'Dell, C., Payne, V. H., Kuai, L., Worden, H. M., Biraud, S. C., Sweeney, C., Stephens, B., Iraci, L. T., Yates, E. L., and Tanaka, T.: Lower-tropospheric CO2 from near-infrared ACOS-GOSAT observations, Atmospheric Chemistry and Physics, 17, 5407–
515 5438, https://doi.org/10.5194/acp-17-5407-2017, 2017.

Kulawik, S. S., O'Dell, C., Nelson, R. R., and Taylor, T. E.: Validation of OCO-2 error analysis using simulated retrievals, Atmospheric Measurement Techniques, 12, 5317–5334, https://doi.org/10.5194/amt-12-5317-2019, 2019.

Lan, X., Tans, P., Sweeney, C., Andrews, A., Jacobson, A., Crotwell, M., Dlugokencky, E., Kofler, J., Lang, P., Thoning, K., and Wolter, S.: Gradients of column CO2 across North America from the NOAA Global Greenhouse Gas Reference Network, Atmospheric Chemistry and Physics, 17, 15 151–15 165, https://doi.org/10.5194/acp-17-15151-2017, 2017.

Lauvaux, T., Ogle, S., Schuh, A. E., Andrews, A., Uliasz, M., Davis, K. J., Denning, A. S., Miles, N., Richardson, S., Lokupitiya, E., West, T. O., and Cooley, D.: Evaluating atmospheric CO 2 inversions at multiple scales over a highly inventoried agricultural landscape , Global Change Biology, 19, 1424–1439, https://doi.org/10.1111/gcb.12141, 2013.

Lin, J. C., Gerbig, C., Wofsy, S. C., Andrews, A. E., Daube, B. C., Davis, K. J., and Grainger, C. A.: A near-field tool for simulating the upstream influence of atmospheric observations: The Stochastic Time-Inverted Lagrangian Transport (STILT) model, Journal of Geophysical Research: Atmospheres, 108, https://doi.org/10.1029/2002jd003161, 2003.

Miller, C. E., Crisp, D., DeCola, P. L., Olsen, S. C., Randerson, J. T., Michalak, A. M., Alkhaled, A., Rayner, P., Jacob, D. J., Suntharalingam, P., Jones, D. B., Denning, A. S., Nicholls, M. E., Doney, S. C., Pawson, S., Boesch, H., Connor, B. J., Fung, I. Y., O'Brien, D., Salawitch, R. J., Sander, S. P., Sen, B., Tans, P., Toon, G. C., Wennberg, P. O., Wofsy, S. C., Yung, Y. L., and Law, R. M.: Precision requirements for space-based XCO2 data, Journal of Geophysical Research Atmospheres, 112, 1–19, https://doi.org/10.1029/2006JD007659, 2007.

Miller, S. M. and Michalak, A. M.: The impact of improved satellite retrievals on estimates of biospheric carbon balance, Atmospheric Chemistry and Physics, 20, 323–331, https://doi.org/10.5194/acp-20-323-2020, doi.org/10.5194/acp-20-323-2020https://acp.copernicus. org/articles/20/323/2020/, 2020.

Nehrkorn, T., Eluszkiewicz, J., Wofsy, S. C., Lin, J. C., Gerbig, C., Longo, M., and Freitas, S.: Coupled weather research and forecasting-stochastic time-inverted lagrangian transport (WRF-STILT) model, Meteorology and Atmospheric Physics, 107, 51–64, https://doi.org/10.1007/s00703-010-0068-x, 2010.

O'Dell, C. W., Connor, B., Bösch, H., O'Brien, D., Frankenberg, C., Castano, R., Christi, M., Eldering, D., Fisher, B., Gunson, M., McDuffie, J., Miller, C. E., Natraj, V., Oyafuso, F., Polonsky, I., Smyth, M., Taylor, T., Toon, G. C., Wennberg, P. O., and Wunch, D.: The ACOS CO2 retrieval algorithm-Part 1: Description and validation against synthetic observations, Atmospheric Measurement Techniques, 5, 99–121, https://doi.org/10.5194/amt-5-99-2012, 2012.

O'Dell, C. W., Eldering, A., Wennberg, P. O., Crisp, D., Gunson, M. R., Fisher, B., Frankenberg, C., Kiel, M., Lindqvist, H., Mandrake, L., Merrelli, A., Natraj, V., Nelson, R. R., Osterman, G. B., Payne, V. H., Taylor, T. E., Wunch, D., Drouin, B. J., Oyafuso, F., Chang, A., McDuffie, J., Smyth, M., Baker, D. F., Basu, S., Chevallier, F., Crowell, S. M., Feng, L., Palmer, D. P. I., Dubey, M., García, O. E., Griffith, D. W., Hase, F., Iraci, L. T., Kivi, R., Morino, I., Notholt, J., Ohyama, H., Petri, C., Roehl, C. M., Sha, M. K., Strong, K., Sussmann, R., Te, Y., Uchino, O., and Velazco, V. A.: Improved retrievals of carbon dioxide from Orbiting Carbon Observatory-2 with the version 8 ACOS algorithm, Atmospheric Measurement Techniques, 11, 6539–6576, https://doi.org/10.5194/amt-11-6539-2018, 2018.

Olsen, S. C.: Differences between surface and column atmospheric CO 2 and implications for carbon cycle research , Journal of Geophysical Research, 109, 1–11, https://doi.org/10.1029/2003jd003968, 2004.

Osterman, G., O'Dell, C., Eldering, A., Fisher, B., Crisp, D., Cheng, C., Frankenberg, C., Lambert, A., Gunson, M. R., Mandrake, L., Wunch, D., and Kiel, M.: Orbiting Carbon Observatory-2 & 3 (OCO-2 & OCO-3): Data Product User's Guide, Operational Level 2 Data Versions 10 and Lite File Version 10 and VEarly, https://doi.org/https://docserver.gesdisc.eosdis.nasa.gov/public/project/OCO/OCO2_OCO3_B10_DUG.pdf, 2020.

Peters, W., Jacobson, A. R., Sweeney, C., Andrews, A. E., Conway, T. J., Masarie, K., Miller, J. B., Bruhwiler, L. M. P., Petron, G., Hirsch, A. I., Worthy, D. E. J., van der Werf, G. R., Randerson, J. T., Wennberg, P. O., Krol, M. C., and Tans, P. P.: An atmospheric perspective

555   on North American carbon dioxide exchange: CarbonTracker, Proceedings of the National Academy of Sciences, 104, 18 925–18 930, https://doi.org/10.1073/pnas.0708986104, http://www.pnas.org/cgi/doi/10.1073/pnas.0708986104, 2007.

Piao, S., Wang, X., Wang, K., Li, X., Bastos, A., Canadell, J. G., Ciais, P., Friedlingstein, P., and Sitch, S.: Interannual variation of terrestrial carbon cycle: Issues and perspectives, Global Change Biology, 26, 300–318, https://doi.org/10.1111/gcb.14884, 10.1111/gcb.14884, 2020.

Potter, C. S., Randerson, J. T., Field, C. B., Matson, P. A., Vitousek, P. M., Mooney, H. A., and Klooster, S. A.: Terrestrial ecosystem
560   production: a process model based on global satellite and surface data, Global Biogeochemical Cycles, 7, 811–841, 1993.

Rayner, P. J. and O'Brien, D. M.: The utility of remotely sensed CO2 concentration data in surface source inversions, Geophysical Research Letters, 28, 175–178, https://doi.org/10.1029/2000GL011912, 2001.

Riebesell, U., Rtzinger, A. K., and Oschlies, A.: Sensitivities of marine carbon fluxes to ocean change, Proceedings of the National Academy of Sciences of the United States of America, 106, 20 602–20 609, https://doi.org/10.1073/pnas.0813291106, 2009.

565   Rödenbeck, C., Zaehle, S., Keeling, R., and Heimann, M.: The European carbon cycle response to heat and drought as seen from atmospheric CO 2 data for 1999–2018, Philosophical Transactions of the Royal Society B: Biological Sciences, 375, 20190 506, https://doi.org/10.1098/rstb.2019.0506, https://royalsocietypublishing.org/doi/10.1098/rstb.2019.0506, 2020.

Schaefer, K., Collatz, G. J., Tans, P., Denning, A. S., Baker, I., Berry, J., Prihodko, L., Suits, N., and Philpott, A.: Combined simple biosphere/carnegie-ames-stanford approach terrestrial carbon cycle model, Journal of Geophysical Research: Biogeosciences, 113, 1–
570   13, https://doi.org/10.1029/2007JG000603, 2008.

Schuh, A. E., Denning, A. S., Uliasz, M., and Corbin, K. D.: Seeing the forest through the trees: Recovering large-scale carbon flux biases in the midst of small-scale variability, Journal of Geophysical Research: Biogeosciences, 114, 1–11, https://doi.org/10.1029/2008JG000842, 2009.

Schuldt, K. N., Mund, J., Luijkx, I. T., Jacobson, A. R., Cox, A., Vermeulen, A., Manning, A., Beyersdorf, A., Manning, A., Karion,
575   A., Hensen, A., Arlyn Andrews, Frumau, A., Colomb, A., Scheeren, B., Law, B., Baier, B., Munger, B., Paplawsky, B., Viner, B., Stephens, B., Daube, B., Labuschagne, C., Myhre, C. L., Hanson, C., Miller, C. E., Plass-Duelmer, C., Sloop, C. D., Sweeney, C., Kubistin, D., Goto, D., Jaffe, D., Say, D., Dinther, D. V., Bowling, D., Dickon Young, Weyrauch, D., Worthy, D., Dlugokencky, E., Gloor, E., Cuevas, E., Reyes-Sanchez, E., Hintsa, E., Kort, E., Morgan, E., Apadula, F., Francois Gheusi, Meinhardt, F., Moore, F., Vitkova, G., Chen, G., Bentz, G., Manca, G., Brailsford, G., Forster, G., Riris, H., Meijer, H., Matsueda, H., Huilin Chen, Levin, I.,
580   Lehner, I., Mammarella, I., Bartyzel, J., Abshire, J. B., Elkins, J. W., Levula, J., Jaroslaw Necki, Pichon, J. M., Peischl, J., Müller-Williams, J., Turnbull, J., Miller, J. B., Lee, J., Lin, J., Josep-Anton Morgui, DiGangi, J. P., Hatakka, J., Coletta, J. D., Holst, J., Kominkova, K., McKain, K., Saito, K., Aikin, K., Davis, K., Thoning, K., Tørseth, K., Haszpra, L., Mitchell, L., Gatti, L. V., Emmenegger, L., Lukasz Chmura, Merchant, L., Sha, M. K., Delmotte, M., Fischer, M. L., Schumacher, M., Torn, M., Leuenberger, M., Steinbacher, M., Schmidt, M., Mazière, M. D., Sargent, M., Lindauer, M., Mölder, M., Martin, M. Y., Shook, M., Galkowski, M., He-
585   liasz, M., Marek, M. V., Ramonet, M., Miroslaw Zimnoch, Lopez, M., N. Mihalopoulos, Miles, N., Laurent, O., Peltola, O., Hermanssen, O., Trisolino, P., Cristofanelli, P., Kolari, P., Krummel, P., Shepson, P., Smith, P., Rivas, P. P., Bakwin, P., Bergamaschi, P., Keronen, P., Tans, P., Bulk, P. V. D., Keeling, R., Ramos, R., Langenfelds, R., Curcoll, R., Commane, R., Newman, S., Hammer, S., Richardson, S., Biraud, S. C., Conil, S., Clark, S., Morimoto, S., Aoki, S., O'Doherty, S., Sites Climadat, Wekker, S. D., Kawa, S. R., Montzka, S., Walker, S., Piper, S., Wofsy, S., Nichol, S., Lauvaux, T., Ryerson, T., Griffis, T., Biermann, T., Machida, T., Lau-
590   rila, T., Aalto, T., Gomez-Trueba, V., Joubert, W., Niwa, Y., Sawa, Y., and Loh, Z.: Multi-laboratory compilation of atmospheric carbon dioxide data for the period 1957-2019; obspack_co2_1_GLOBALVIEWplus_v6.0_2020-09-11, https://doi.org/10.25925/20200903, https://www.esrl.noaa.gov/gmd/ccgg/obspack/data.php?id=obspack_co2_1_GLOBALVIEWplus_v6.0_2020-09-11, 2020.

Atmospheric
Chemistry
and Physics
Discussions
Open Access
EGU

Sweeney, C., Karion, A., Wolter, S., Newberger, T., Guenther, D., Higgs, J. A., Andrews, A. E., Lang, P. M., Neff, D., Dlugokencky, E., Miller, J. B., Montzka, S. A., Miller, B. R., Masarie, K. A., Biraud, S. C., Novelli, P. C., Crotwell, M., Crotwell, A. M., Thoning, K., and

595   Tans, P. P.: Journal of Geophysical Research : Atmospheres, pp. 5155–5190, https://doi.org/10.1002/2014JD022591.Received, 2015.

Takagi, H., Houweling, S., Andres, R. J., Belikov, D., Bril, A., Boesch, H., Butz, A., Guerlet, S., Hasekamp, O., Maksyutov, S., Morino, I., Oda, T., O'Dell, C. W., Oshchepkov, S., Parker, R., Saito, M., Uchino, O., Yokota, T., Yoshida, Y., and Valsala, V.: Influence of differences in current GOSAT X CO 2 retrievals on surface flux estimation, Geophysical Research Letters, 41, 2598–2605, https://doi.org/10.1002/2013GL059174, http://doi.wiley.com/10.1002/2013GL059174, 2014.

600   Tans, P. P., Conway, T. J., and Nakazawa, T.: Latitudinal distribution of the sources and sinks of atmospheric carbon dioxide derived from surface observations and an atmospheric transport model, Journal of Geophysical Research, 94, 5151–5172, https://doi.org/10.1029/JD094iD04p05151, 1989.

Tans, P. P., Fung, I. Y., and Takahashi, T.: Observational constraints on the global atmospheric CO2 budget, Science, 247, 1431–1438, https://doi.org/10.1126/science.247.4949.1431, 1990.

605   Wofsy, S. C., Wofsy, S. C., Harriss, R. C., and Harriss, R. C.: The NACP Committee of the U.S. Carbon Cycle Science Steering Group, Program, p. 62, 2002.

Wu, J., Kobayashi, H., Stark, S. C., Meng, R., Guan, K., Tran, N. N., Gao, S., Yang, W., Restrepo-Coupe, N., Miura, T., Oliviera, R. C., Rogers, A., Dye, D. G., Nelson, B. W., Serbin, S. P., Huete, A. R., and Saleska, S. R.: Biological processes dominate seasonality of remotely sensed canopy greenness in an Amazon evergreen forest, New Phytologist, 217, 1507–1520, https://doi.org/10.1111/nph.14939,

610   2018.

Wunch, D., Toon, G. C., Wennberg, P. O., Wofsy, S. C., Stephens, B. B., Fischer, M. L., Uchino, O., Abshire, J. B., Bernath, P., Biraud, S. C., Blavier, J. F., Boone, C., Bowman, K. P., Browell, E. V., Campos, T., Connor, B. J., Daube, B. C., Deutscher, N. M., Diao, M., Elkins, J. W., Gerbig, C., Gottlieb, E., Griffith, D. W., Hurst, D. F., Jiménez, R., Keppel-Aleks, G., Kort, E. A., MacAtangay, R., MacHida, T., Matsueda, H., Moore, F., Morino, I., Park, S., Robinson, J., Roehl, C. M., Sawa, Y., Sherlock, V., Sweeney, C., Tanaka, T., and Zondlo,

615   M. A.: Calibration of the total carbon column observing network using aircraft profile data, Atmospheric Measurement Techniques, 3, 1351–1362, https://doi.org/10.5194/amt-3-1351-2010, 2010.

Wunch, D., Wennberg, P. O., Toon, G. C., Connor, B. J., Fisher, B., Osterman, G. B., Frankenberg, C., Mandrake, L., O'Dell, C., Ahonen, P., Biraud, S. C., Castano, R., Cressie, N., Crisp, D., Deutscher, N. M., Eldering, A., Fisher, M. L., Griffith, D. W., Gunson, M., Heikkinen, P., Keppel-Aleks, G., Kyrö, E., Lindenmaier, R., MacAtangay, R., Mendonca, J., Messerschmidt, J., Miller, C. E., Morino, I., Notholt, J.,

620   Oyafuso, F. A., Rettinger, M., Robinson, J., Roehl, C. M., Salawitch, R. J., Sherlock, V., Strong, K., Sussmann, R., Tanaka, T., Thompson, D. R., Uchino, O., Warneke, T., and Wofsy, S. C.: A method for evaluating bias in global measurements of CO 2 total columns from space, Atmospheric Chemistry and Physics, 11, 12 317–12 337, https://doi.org/10.5194/acp-11-12317-2011, 2011.

Wunch, D., Toon, G. C., Sherlock, V., Deutscher, N. M., Liu, C., Feist, D. G., and Wennberg, P. O.: The Total Carbon Column Observing Network's GGG2014 Data Version, Tech. rep., California Institute of Technology, Pasadena,

625   CA, https://doi.org/10.14291/tccon.ggg2014.documentation.R0/1221662, http://dx.doi.org/10.14291/tccon.ggg2014.documentation.R0/1221662, 2015.

Wunch, D., Wennberg, P. O., Osterman, G., Fisher, B., Naylor, B., Roehl, M. C., O'Dell, C., Mandrake, L., Viatte, C., Kiel, M., Griffith, D. W., Deutscher, N. M., Velazco, V. A., Notholt, J., Warneke, T., Petri, C., De Maziere, M., Sha, M. K., Sussmann, R., Rettinger, M., Pollard, D., Robinson, J., Morino, I., Uchino, O., Hase, F., Blumenstock, T., Feist, D. G., Arnold, S. G., Strong, K., Mendonca, J., Kivi, R.,

630   Heikkinen, P., Iraci, L., Podolske, J., Hillyard, P., Kawakami, S., Dubey, M. K., Parker, H. A., Sepulveda, E., García, O. E., Te, Y., Jeseck,

P., Gunson, M. R., Crisp, D., and Eldering, A.: Comparisons of the Orbiting Carbon Observatory-2 (OCO-2) XCO2 measurements with
TCCON, Atmospheric Measurement Techniques, 10, 2209–2238, https://doi.org/10.5194/amt-10-2209-2017, 2017.

York, D., Evensen, N. M., Martı´nez, M. L., and De Basabe Delgado, J.: Unified equations for the slope, intercept, and standard errors of the
best straight line, American Journal of Physics, 72, 367–375, https://doi.org/10.1119/1.1632486, 2004.